Temperature Dependence of the Reconstruction of Zigzag Edges in Graphene

Kuang He,[†] Alex W. Robertson,[†] Ye Fan,[†] Christopher S. Allen,[†] Yung-Chang Lin,[‡] Kazu Suenaga,[‡] Angus I. Kirkland,[†] and Jamie H. Warner*,[†]

[†]Department of Materials, University of Oxford, Parks Road, Oxford OX1 3PH, U.K. and [‡]Nanotube Research Center, Advanced Institute for Industrial Science and Technology, Tsukuba 305-8561, Japan

ABSTRACT We examine the temperature dependence of graphene edge terminations at the atomic scale using an *in situ* heating holder within an aberration-corrected transmission electron microscope. The relative ratios of armchair, zigzag, and reconstructed zigzag edges from over 350 frames at each temperature are measured. Below 400 °C, the edges are dominated by zigzag terminations, but above 600 °C, this changes dramatically, with edges dominated by armchair and reconstructed zigzag edges. We show that at low temperature chemical etching effects dominate and cause deviation to the thermodynamics of the system. At high temperatures (600 and 800 °C), adsorbates are evaporated from the surface of graphene and chemical etching effects are significantly reduced, enabling the thermodynamic distribution of edge types to be observed. The growth rate of holes at high temperature is also shown to be slower than at room temperature, indicative of the reduced chemical etching process. These results provide important insights into the role of chemical etching effects in the hole formation, edge sputtering, and edge reconstruction in graphene.

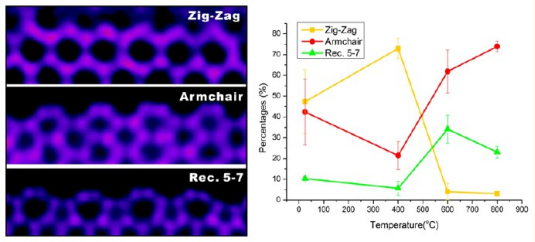

KEYWORDS: graphene · edges · high temperature · HRTEM · reconstructed zigzag

The structure of edges in graphene has a great influence on its mesoscopic properties.[1−7] Nanoconstraint structures in graphene such as nanoribbons,[8,9] quantum dots,[10] and nanojunctions[11−13] are largely influenced by the edge configurations due to the high edge/bulk ratio. Experimental studies of graphene edges typically use either scanning tunneling microscopy,[9,14−17] aberration-corrected transmission electron microscopy (AC-TEM),[18−21] or micro-Raman spectroscopy.[22,23] Despite the abundant studies and structural characterization carried out on the geometry of edge structures, being able to control the edge termination freely still remains a challenging topic. Most top-down production techniques such as electron and photolithography, unzipping of carbon nanotubes, and metal-particle-assisted etching result in defective graphene edges.[8,24−27] Anisotropic etching of graphene with the assistance of metal nanoparticles and hydrogen at elevated temperatures has been reported recently to produce predominately zigzag edges,[28,29] but characterization of these edges at the atomic scale is lacking. While graphene edges might appear regular at the micrometer scale, often closer examination at the detailed atomic level reveals more complex edge terminations that are not fully periodic.[30,31] Tearing graphene has been shown to be one approach for achieving long periodic edge structures.[33]

The three main periodic edge terminations of graphene are presented in Figure 1. The armchair configuration shown in Figure 1a,b and the zigzag configuration shown in Figure 1c,d have long been recognized as the intrinsic edges of graphene. Both types can also reconstruct into different geometries. For example, zigzag edges are known to reconstruct into a pentagon−heptagon structure (namely, Rec. 5−7 edges) through a series of bond rotations, shown in Figure 1e,f, to lower its energy.[32−34] There is no atom loss involved with this process, as can be seen from Figure 1g−i; one C−C bond rotates 90° and rebonds to the nearest atom after rotation. This is similar to the

* Address correspondence to jamie.warner@materials.ox.ac.uk.

Received for review February 18, 2015 and accepted April 10, 2015.

Published online April 16, 2015
10.1021/acsnano.5b01130

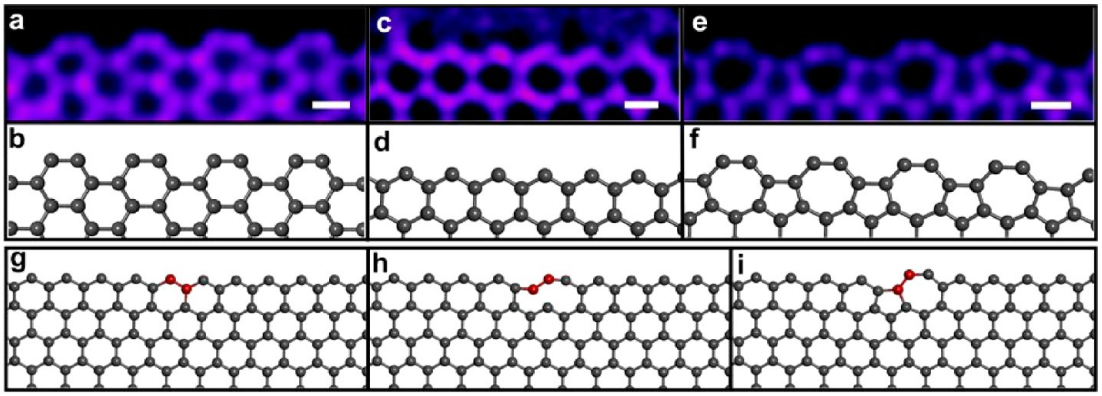

Figure 1. Three periodic edge terminations of graphene. (a) AC scanning TEM (AC-STEM) image of an armchair edge and (b) its atomic model. (c) AC-TEM image of a zigzag edge and (d) its atomic model. (e) AC-STEM image of a reconstructed 5−7 edge and (f) its atomic model. (g−i) Schematic illustration showing the reconstruction process from zigzag to the Rec. 5−7 edge; atoms highlighted in red are the rotated atoms. All scale bars are 0.2 nm.

Stone−Wales bond rotation in the bulk of graphene.[35] Armchair edges have two reconstructed forms, a hexagon−heptagon−heptagon structure (namely, ac(677)) and a pentagon−hexagon structure (namely, ac(56)).[36] Both of which, according to computational results, have higher energy than the original unreconstructed form, and for that reason, no long-ordered structures of these configurations have been observed experimentally; they only appear as isolated incidents on an occasional basis.[32,34,36]

Koskinen *et al.* studied the theoretical geometry and energy of graphene edges and predicted that armchair, zigzag, and Rec. 5−7 have edge energies of 2.09, 3.22, and 2.36 eV/atom, respectively.[36] A recent report showed that, under electron beam irradiation at an accelerating voltage of 300 kV and at high temperatures of 700 °C, armchair edges became the major edge termination of graphene.[37] A similar result was observed by Joule heating a graphene sample to even higher temperatures using an *in situ* electrical holder inside an AC-TEM at a lower accelerating voltage of 80 kV.[41] However, not much attention has been paid to the fine details of the temperature dependence of zigzag edges, in particular, determining the crossover temperature where the low-energy Rec. 5−7 edge dominates over the zigzag edge. At room temperature, zigzag edges are far more prevalent than the Rec. 5−7 edge when being observed using AC-TEM, and this was attributed to their higher stability under electron beam irradiation.[19] Even though the Rec. 5−7 edge has lower energy than the zigzag edge, a small energy barrier must be overcome for this transition to occur, in the same way a Stone−Wales bond rotation requires overcoming an energy barrier. A single Stone−Wales rotation within a bulk graphene sheet was estimated to have a formation energy of 5.08 eV, after overcoming the initial ∼10 eV barrier.[38] At the edge, this is reduced to ∼1.1 eV because one of the atoms involved with the rotation is only bonded to two other atoms; therefore, less bonds need to be broken.[33] At a certain temperature, the thermal energy provided to the system might be large enough to overcome this lower barrier of bond rotation at the edge, and this would then result in the zigzag edge flipping to its Rec. 5−7 form. Density functional tight binding calculation predicts that, under 80 keV electron beam sputtering, the armchair structure has the highest radiation stability, followed by Rec. 5−7 and zigzag configuration.[39] With residual contamination, such as from amorphous carbon, metal particles are known to remain on the surface of graphene from the synthesis and transfer process. Heating of the sample would dissipate the contamination and prevent the chemical etching effect under continuous electron beam irradiation, revealing the accurate graphene edge behavior under an electron beam.

RESULTS AND DISCUSSION

Here, we explore this by adjusting the temperature of graphene in steps from room temperature to 800 °C using an *in situ* heating holder within an aberration-corrected TEM. Atomic resolution images of the edges of holes in graphene enable us to determine the statistical ratio of the three different edge terminations. The holes are intentionally created in graphene using a controlled focused electron beam sputtering method. This approach for hole creation is well-established and has been previously reported.[40] We allowed the holes to grow in size until they reached at least 15 nm in size to ensure individual edge lengths around the hole were long enough to have statistical meaning.

Figure 2 shows the results at room temperature (∼25 °C). Figure 2a−c shows three different representative holes, with the edges being color-coded according to different edge terminations. The insets in Figure 2a,b provide atomic models of the zigzag and armchair edges observed in these regions. The room temperature statistics (Figure 2d) for all three time series of different holes show that ∼45% are zigzag, ∼40% are armchair, and ∼10% are Rec. 5−7.

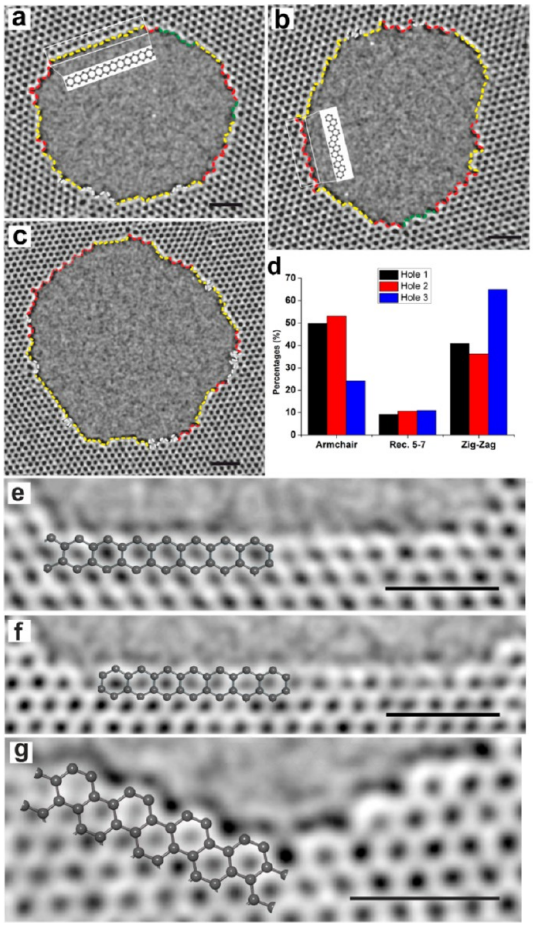

Figure 2. Edge behavior at room temperature (~25 °C). (a–c) Three typical HRTEM images of graphene holes at that temperature. The edges are color-coded to differentiate the types of edge configurations. Red represents armchair; yellow is zigzag, and green is Rec. 5–7; white indicates mixed or unidentified edge types. The inset in (a) and (b) shows typical long-ordered zigzag and armchair configurations at this temperature. The statistics for three examples are shown in (d); the percentages of edges occupied by different types of edges are ranked accordingly: black columns represent panel (a), red columns panel (b), and blue columns panel (c). (e,f) Long-ordered zigzag edge from both bulk of graphene and edge of a nanoribbon, respectively. (g) Representative long-ordered armchair edge found at this temperature. The original image of which (e–g) are cropped from those shown in Figure S1a–c of Supporting Information. All scale bars are 1 nm.

Typical long-ordered zigzag edges are shown in Figure 2e,f and a long-ordered armchair edge in Figure 2g.

Increasing the temperature to 400 °C did not change the distribution of edge terminations significantly, as shown in Figure 3. Three typical holes are shown in Figure 3a–c, together with the statistics for three time series of different holes shown in Figure 3d. Zigzag edges still form ~70%, armchair ~20%, and Rec. 5–7 <5%. Figure 3e shows a typical long-ordered zigzag structure and again is generally longer than the armchair edges shown in Figure 3f. This shows that the edge structure of graphene at 400 °C is similar to that at 25 °C.

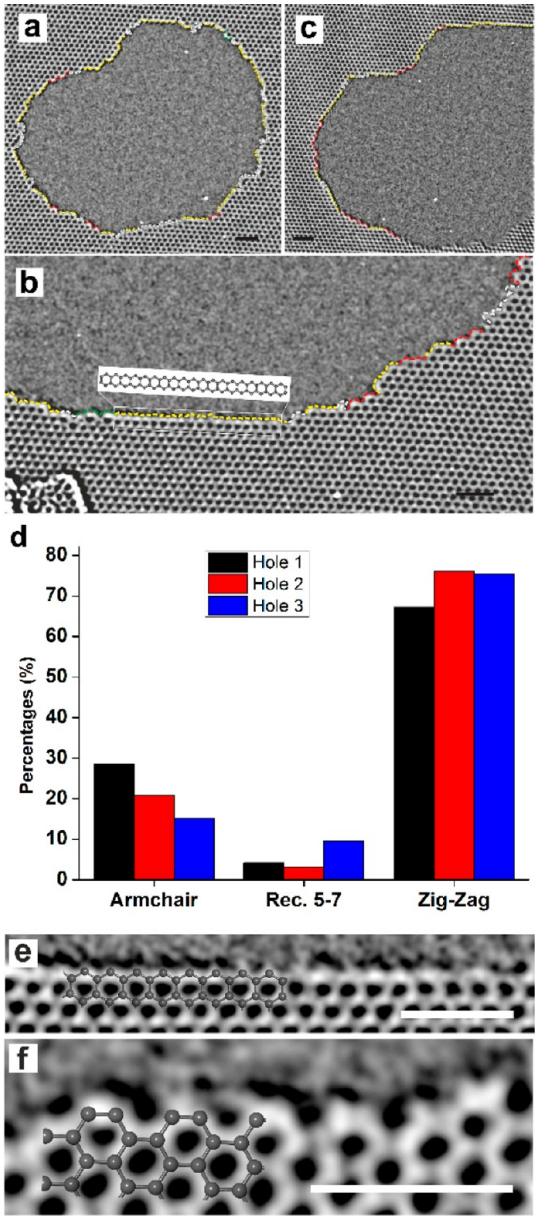

Figure 3. Edge behavior at 400 °C. (a–c) Three typical HRTEM images of graphene holes at this temperature. The edges are color-coded to differentiate the types of edge configurations. Red represents armchair; yellow is zigzag, and green is Rec. 5–7; white indicates mixed or unidentified edge types. The inset in (c) shows that a typical long-ordered zigzag configuration occurred at this temperature. The statistics for three examples are shown in panel (d); the percentages of edges occupied by different types of edges are ranked accordingly: black columns represent panel (a), red columns panel (b), and blue columns panel (c). (e) Representative long-ordered zigzag edge cropped from panel (c) and zoomed in. (f) Representative long-ordered armchair edge cropped from panel (b) and zoomed in. All scale bars are 1 nm.

Increasing the temperature to 600 °C resulted in a drastically different distribution of edge terminations, shown in Figure 4. Armchair edges now account for ~60%, zigzag <5%, and Rec. 5–7 30–40%. The major change is the large decrease in the percentage of zigzag edges at the expense of a rise in Rec. 5–7

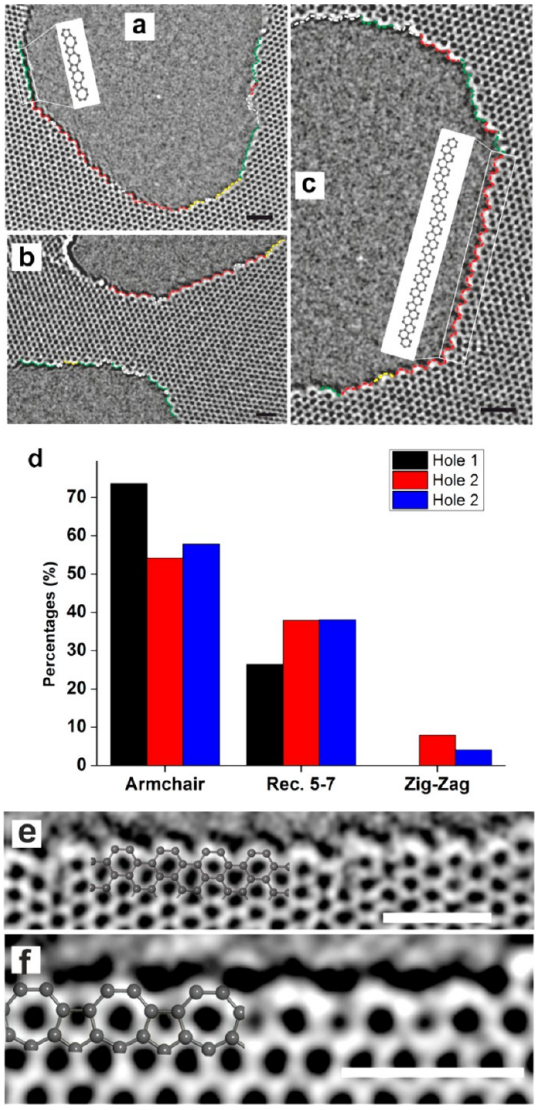

Figure 4. Edge behaviors at 600 °C. (a–c) Three typical HRTEM images of graphene holes at this temperature. The edges are color-coded to differentiate the types of edge configurations. Red represents armchair; yellow is zigzag, and green is rec. 5–7; white indicates mixed or unidentified edge types. The inset in (a) and (c) shows typical long-ordered reconstructed 5–7 and armchair configurations at this temperature. The statistics for three examples are shown in (d); the percentages of edges occupied by different types of edges are ranked accordingly: black columns represent panel (a), red columns panel (b), and blue columns panel (c). (e) Representative long-ordered armchair edge cropped from panel (c) and zoomed in. (f) Representative long-ordered Rec. 5–7 edge cropped from panel (a) and zoomed in. All scale bars are 1 nm.

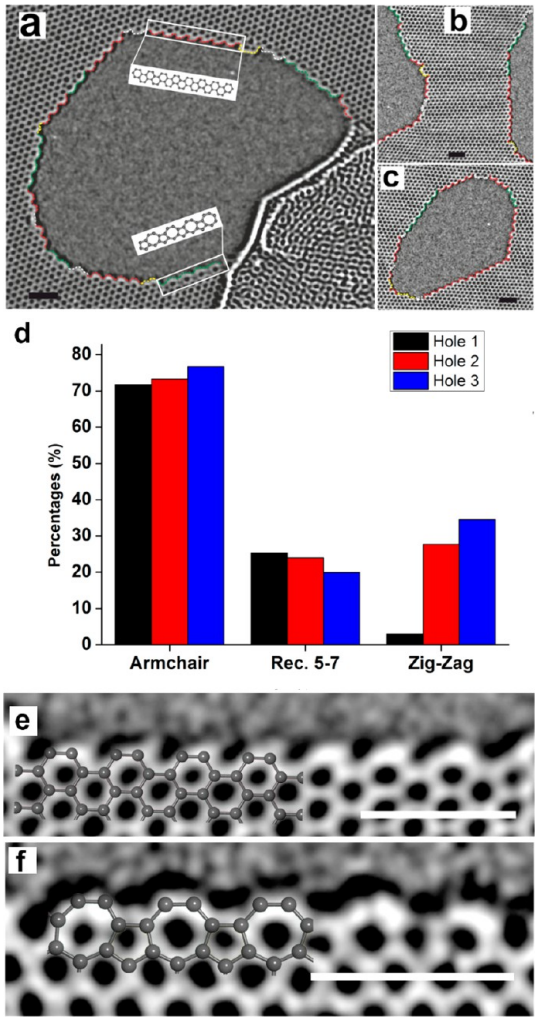

Figure 5. Edge behaviors at 800 °C. (a–c) Three typical HRTEM images of graphene holes at this temperature. The edges are color-coded to differentiate the types of edge configurations. Red represents armchair; yellow is zigzag, and green is Rec. 5–7; white indicates mixed or unidentified edge types. The inset in (a) shows typical long-ordered Rec. 5–7 and armchair configurations at this temperature. The statistics for three examples are shown in panel (d), and the percentages of different types of edges are ranked accordingly: black columns represent panel (a), red columns panel (b), and blue columns panel (c). (e) Representative long-ordered armchair edge cropped from panel (c) and zoomed in. (f) Representative long-ordered Rec. 5–7 edge cropped from panel (a) and zoomed in. All scale bars are 1 nm.

edges. The inset of Figure 4a shows the long-ordered Rec. 5–7 edges, and the inset of Figure 4c shows the long-ordered armchair edge. No long-ordered zigzag edge structure was observed. A typical long-ordered armchair structure is shown at higher magnification in Figure 4e, and the length is longer than those obtained at room temperature and 400 °C. Long-ordered Rec. 5–7 structures, such as those seen Figure 4f, start to appear more frequently. Observation of edge structures is carried out at various time periods after temperature increase, ranging from 10 min to overnight heating. The surface adsorbates are found to be evaporated immediately, and no significant change of the adsorbates density in terms of heating time was observed. The edge structure was also found to be independent of heating time—the edge configurations do not experience significant change after overnight heating.

Finally, we increased the temperature to 800 °C to examine if any further changes occurred to the distribution of edge types, shown in Figure 5. Along the

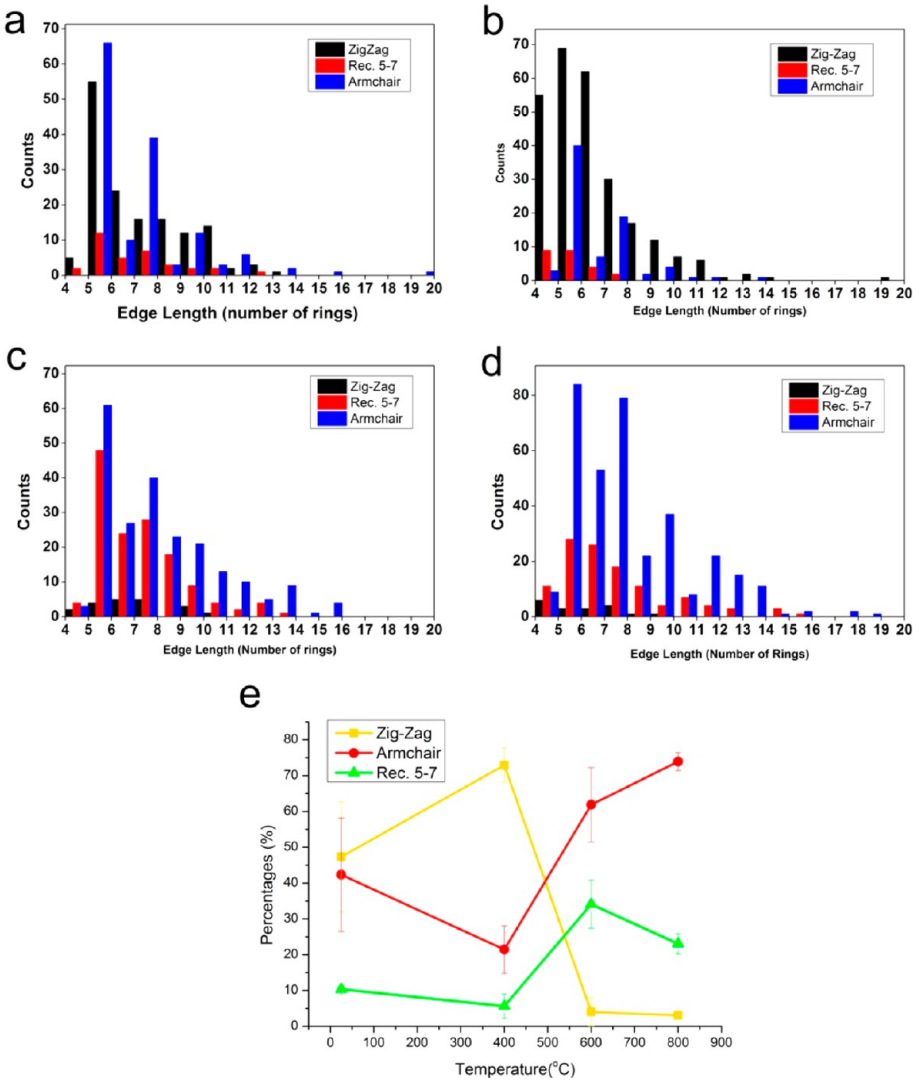

Figure 6. Statistics of edge configurations at various temperatures. (a−d) Statistics of edge configuration at RT, 400, 600, and 800 °C, respectively. The number of occurrences is plotted against the edge length (number of rings that makes up the edge). (e) Three trend lines represent the temperature dependency of different edge configurations: yellow for zigzag, red for armchair, and green for reconstructed 5−7. The percentage of each edge type is calculated by dividing the sum of edge length of this type by the total number of edges counted.

long armchair edge on the upper left corner of Figure 5a, a 7−5−7 edge structure occurred and along the same direction as the armchair edge. This occurs from reconstruction of a near edge defect, instead of zigzag reconstruction. This type of reconstruction is short-range and is not likely to affect the overall statistics. The statistics in Figure 5d show that armchair remains the most predominate edge at ∼70% followed by Rec. 5−7 edge (20−30%), with the zigzag edge being the least frequently observed edge type (<5%), similar to the case at 600 °C. Figure 5e,f shows typical examples of armchair and Rec. 5−7 edges at this temperature. The absence of any further changes in the edge distributions indicates that the region between 400 and 600 °C is the major point of interest.

More than 350 frames like the ones shown above taken over multiple number of holes (three holes for each temperature) are then used in the statistical analysis of edge type. The results are shown in Figure 6a−d for room temperature (RT), 400, 600, and 800 °C, respectively. Only holes with diameters larger than ∼15 nm are included in the counting process to keep the edge strain effect to a minimum. Also, only edges that have four rings or longer are considered. The maximum counts occur for the edge length of ∼6 rings for all four temperatures, with the counts tailing off toward longer edge lengths. The most perceptible difference between low temperature (RT and 400 °C, a,b) and high temperature (600 and 800 °C, c,d) is the decrease in the number of zigzag edges and increase in the number of armchair and Rec. 5−7 edges. This is summarized in Figure 6e, where the temperature dependence of the average population distribution of the three edge types is plotted. It shows that the major change lies between 400 and 600 °C, where the edges undergo abrupt transformations: zigzag edges

experienced a reduction from ~60 to ~5%, armchair edges increased from ~30 to ~60%, and Rec. 5−7 edges increased from ~5 to ~30%. This shows that the temperature between 400 and 600 °C is the crossover point for zigzag edges converting to Rec. 5−7 edges.

The theoretical formation energy for graphene edge types decreases from zigzag, armchair, to Rec. 5−7.[32,36,41,42] This means the thermodynamic stability should be increasing from zigzag, armchair, to Rec. 5−7. However, within the TEM, edges are irradiated by the electron beam, and radiation stability of the edge is extremely important. Calculations indicate the radiation stability of edges reduces from armchair, Rec. 5−7, to zigzag, which is different than the formation energy.[39] Both armchair and Rec. 5−7 edges have two atoms at the edge that are only bonded to two other atoms; the neighboring two atoms form a dimer, and the kinetic energy provided by the electron collision is distributed between the dimer and occasionally results in a 180° rotation (flipping).[39] The zigzag edge, on the other hand, does not allow this kind of rotational reconstruction due to the geometrical restrictions and is therefore the least stable structure out of the three under electron beam irradiation. Calculations of the sputtering threshold of graphene edges indicate that the edges should be much more stable than current observations reveal.[37,39] It is therefore suggested that the rapid sputtering rate at room temperature of graphene holes is due to a chemical etching process, which essentially lowers the energy threshold of atom removal.

The large change between the low temperature (RT and 400 °C) and high temperature (600 and 800 °C) results is related to both electron-beam-induced sputtering effects and the thermodynamic low-energy structure. Graphene is typically covered with surface adsorbates that remain attached until heated to approximately 500 °C inside the TEM, when they evaporate off and leave a pristinely clean graphene surface. This also influences the concentration of surface chemical species that dictate the chemical etching process of graphene edges. The growth rate of holes in graphene at both RT and 800 °C is shown in Figure S2 of Supporting Information. Holes grow twice as fast at RT compared to 800 °C in our experiment, indicating a decrease in the chemical etching effect at high temperature due to the reduced adsorbate concentration on the surface. During the hole fabrication process, the electron beam is contracted down to a 10 nm spot to maximize the beam current density, and it takes noticeably longer to create a hole using this method at 800 °C (10 min) compared to RT (3 min), supporting the notion that the hole fabrication/growth process at low temperature (below 400 °C) is dominated by chemical etching, activated by large concentration of surface contamination, which might include metal particles, hydrocarbons, and amorphous carbon. The chemical etching effect diminishes as the contamination evaporates off with increasing temperature. The 600 and 800 °C statistics are least effected by chemical etching and reflect the theoretical predictions of edge stability. Long edges are more stable at these high temperatures, illustrated by the larger number of edges with 9−16 rings. The zigzag edge has previously been reported as a predominant edge at room temperature during TEM studies.[19,43] Armchair edges are reported to be more abundant during current annealing with an effective temperature of 2000 K inside the TEM.[37,44] However, these data are based on only a couple of frames and a small number of statistics. Our study tries to address this issue specifically by studying an extensive database (~1400 frames) that covers a full range of temperatures up to 800 °C.

Fully understanding the statistics of edge types at different temperatures requires consideration of the dynamics and lifetime of the edge. It is reported that the zigzag edge reconstructs into the Rec. 5−7 *via* a series of bond rotations driven by electron beam impacts.[33] Prior work showed that graphene torn along the zigzag direction had an edge termination that was stable against electron beam sputtering for about ~50 frames (65 s) and enabled flipping rates from (zigzag → Rec. 5−7) of 0.26 s^{-1} and (Rec. 5−7 → zigzag) of 0.12 s^{-1}.[33] In our experiments at low temperature (RT and 400 °C), the edge configuration changes on a frame-to-frame basis due to the enhanced sputtering from chemical etching, illustrated in Figure 7a,b; the blue dashed lines indicate the number of atoms being etched away. By 95 s at RT and 70 s at 400 °C, one row of zigzag atoms has been removed. Most of the zigzag edges are being etched away without having time to reconstruct, with only a small proportion remaining long enough to reconstruct into the Rec. 5−7 configuration. Furthermore, the sputtering of atoms from a Rec. 5−7 is found to often lead to the transformation back into a zigzag edge and reduces its contribution to the edge distribution statistics.

At high temperature (600 and 800 °C), shown in Figure 7c,d, the outermost row of atoms remained stable for 557 and 173 s, respectively, and the observation of the zigzag edge was only for one frame, making its lifetime extremely short compared to that of the Rec. 5−7. Whereas for the low-temperature measurements, <400 °C, both edge states can be imaged for multiple frames, indicating much longer lifetimes. This can be understood by the mechanisms behind the flipping process. Below 400 °C, the edges are flipped back and forth by electron impacts from the beam, causing bond rotations. This is a stochastic process and would occur equally for both low-temperature and high-temperature measurements, but for the case of temperatures above 600 °C, any time that the electron impacts flip the edge from Rec. 5−7 to zigzag the

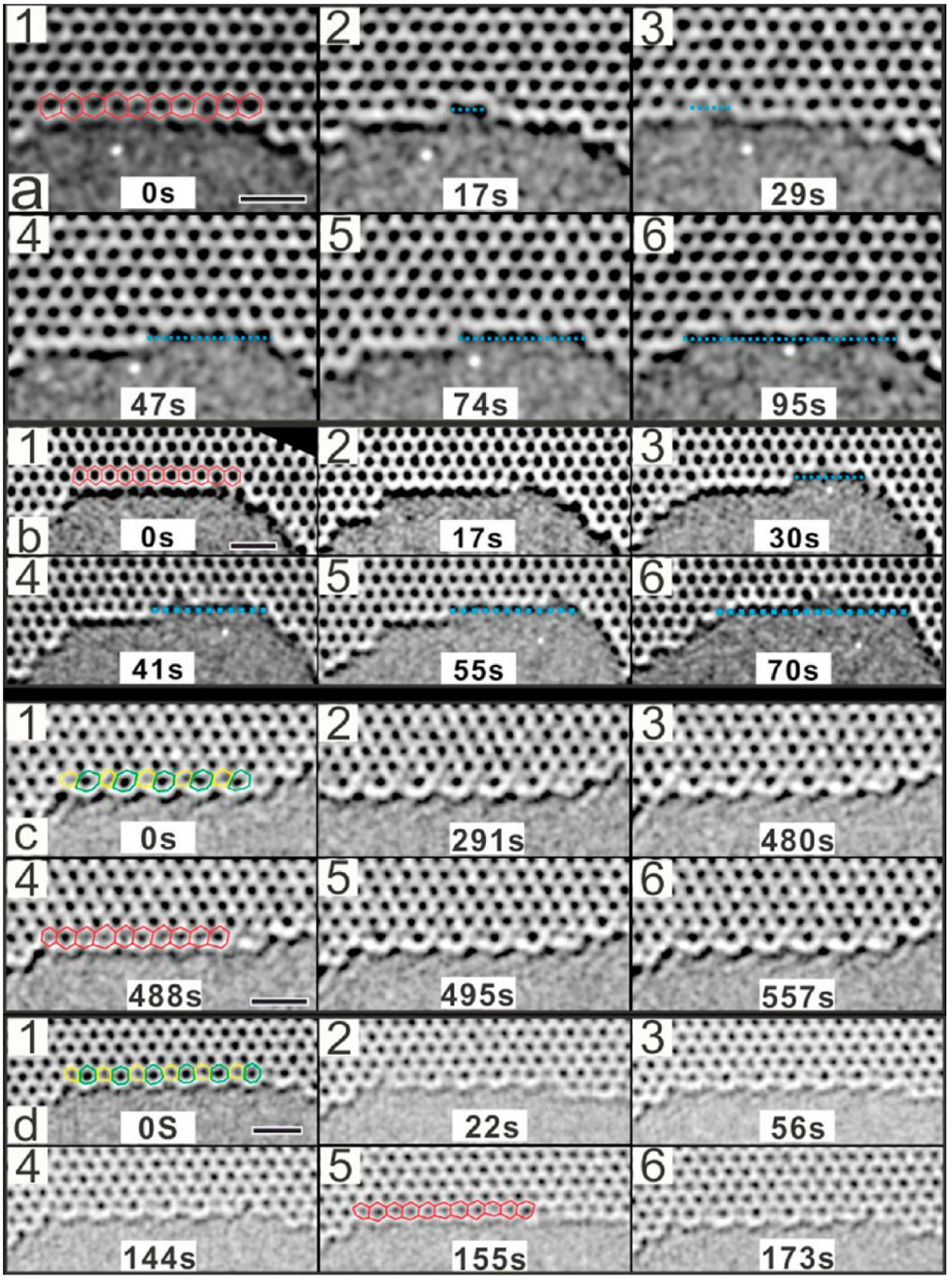

Figure 7. Temperature-dependent edge etching effect. Red, yellow, and green solid lines represent hexagon, pentagon, and heptagon, respectively. The blue dashed lines indicate the row of carbons being lost due to electron sputtering. (a–d) Six time series frames of the same region of the graphene edge at RT, 400, 600, and 800 °C, respectively. All scale bars = 1 nm.

thermal energy in the system rapidly flips it back to Rec. 5–7, giving rise to a short lifetime of zigzag edges. It is likely that the edge flipping process happens many times for the high-temperature measurements; it is simply the case that it does not remain long enough in that state to image, and we cannot capture it. The edge flipping process happens on a much faster time scale than our image acquisition time.

As the temperature increases to 600 and 800 °C, the chemical etching effect weakens dramatically and edge structure is much more stable. Combining with the effect temperature has on the flipping rate explained above, the zigzag edges therefore have enough time to reconstruct into a more stable configuration at these two higher temperatures and result in a higher relative Rec. 5–7 ratio in the statistics. Refererence 33 shows a very special occasion at room temperature where the graphene is extremely clean around the edge area and no sputtering (atom loss) occurred during the entire reconstruction process,

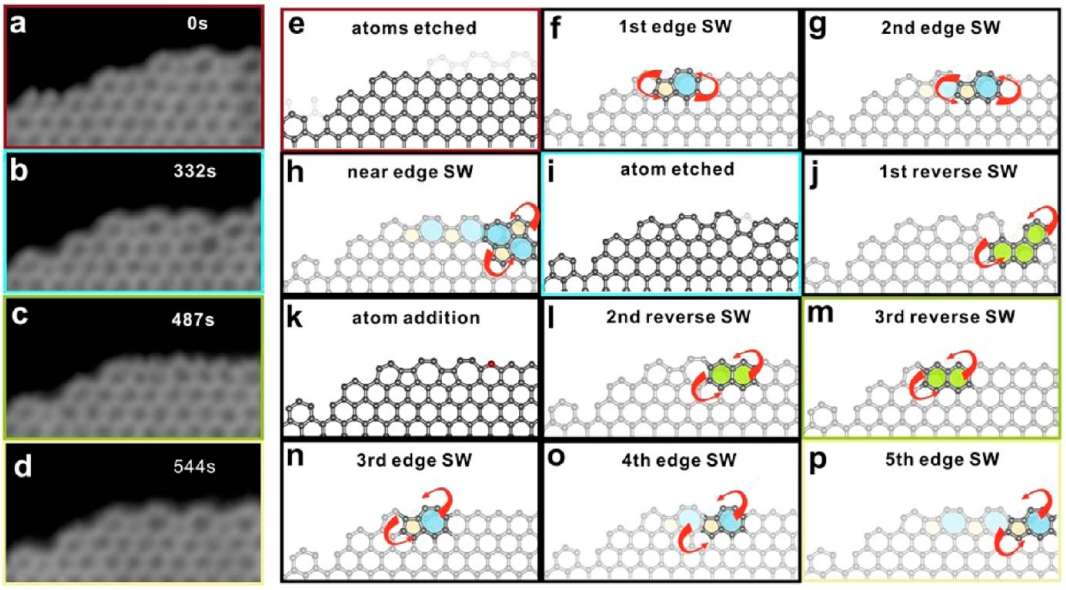

Figure 8. STEM study of zigzag and Rec. 5−7 switching at 550 °C. (a−d) Time sequencing STEM images of graphene edges first being etched and then transformed into Rec. 5−7 configuration. (e−p) Atomic models illustrating the reconstruction process shown in the STEM images. Carbon rings are highlighted to different colors in order to differentiate six-membered rings (green), five-membered rings (yellow), and seven-membered rings (blue). The red arrows demonstrate the direction of Stone−Wales rotation. The atomistic model that is outlined with different colors corresponds to the same atomic structure shown in the STEM image that is outlined with the same color.

essentially emulating the high-temperature behavior in our experiment. Our experiment attempts to generalize the statistics to reflect the edge behavior under all conditions, including the sputtering effect; therefore, more than 1400 frames are used in the statistics.

Probing graphene edges at high temperature using AC-STEM may provide further insights because the STEM probe slowly raster-scans across the sample, rather than illuminating the entire edge as done in phase-contrast HRTEM (Figures 2−7). Flipping an entire long edge from Rec. 5−7 to zigzag at high temperature requires multiple bond rotations, likely induced by multiple sequential electron scattering events. We expect that any local bond rotation randomly induced by the STEM beam will quickly relax back by the time the STEM probe reaches the next section of the edge, and therefore, the edges should be stable Rec. 5−7 structures. Figure 8 shows an example, at 550 °C, where we see transitions between Rec. 5−7 and zigzag, initiated by atom sputtering at the edge (Figure 8b,c). However, it quickly relaxes back to Rec. 5−7 as expected and remains stable in this configuration (Figure 8c,d). Atomic models in Figure 8e−p schematically illustrate the structural transitions occurring between the STEM images.

CONCLUSIONS

AC-TEM imaging of graphene edges has been carried out at four different temperatures (room temperature, 400, 600, and 800 °C). The statistical results show a dramatic transformation of edges between 400 and 600 °C; armchair became the predominant termination structure rather than zigzag, and the Rec. 5−7 edge type also increased. This is caused by a combination effect of the reduction in chemical etching and increase in the flipping rate. The statistics of edge configuration at high temperature (600 and 800 °C) therefore represent the true radiation stability order and agrees with theoretical calculations in the literature. We have also carried out a STEM study of the detailed atom movements involved with this reconstruction process. This temperature-dependent study of graphene edges provides insight into graphene edges on atomic scale and will shed light on future study of graphene nanostructure where edges become a major influence on its physical properties.

EXPERIMENTAL METHODS

Synthesis and Transfer of Graphene. The graphene samples were grown by chemical vapor deposition, using a liquid copper catalyst as previously reported.[45] This was achieved by placing a high-purity copper sheet (Alfa Aesar, Puratonic 99.999% pure, 0.1 mm thick, ~1 cm^2) on top of a similar sized piece of tungsten (Alfa Aesar, 99.95% pure, 0.1 mm thick). This was loaded into the quartz tube of the split-tube to vacuum and filled with argon. The gas flow was set to 100 sccm H_2/Ar (20% gas mix) and 200 sccm pure Ar, and the furnace was ramped to 1090 °C, whereupon the sample was slid into the hot zone of the furnace. The sample was annealed for 30 min, after which the CH_4 flow (1% gas mix in Ar) was set at 10 sccm and the H_2/Ar flow reduced from 100 to 80 sccm while being maintained for 90 min to obtain continuous film growth. The temperature was then

reduced to 1060 °C to allow the copper to solidify; a CH_4 flow was then reintroduced for 30 min to allow graphene to grow within cracks induced during the solidification process. After this, the CH_4 flow was disabled and the sample immediately removed from the furnace hot zone, allowing for rapid cooling in the H_2 and Ar atmosphere.

PMMA (8 wt % in anisole, 495 molecular weight) was spin-coated onto the graphene side of the sample at 4700 rpm for 60 s and then cured at 180 °C for 90 s. The underlying tungsten was electrochemically etched away by attaching the sample to the anode and being fully immersed in 1 M of sodium hydroxide solution. The copper was removed by floating the remaining samples in 1 M of ammonia persulfate solution, until just a transparent PMMA/graphene film remained suspended on the surface. This was then cleaned by floating on fresh DI water three times for 10 min each time. The film was then transferred to a prefabricated heating holder (DENS Solutions DENS-C-30). After being left to dry for about 3 h, the sample was baked on a hot plate for 15 min to remove water and improve sample adhesion with the wafer. The sample was then placed in a furnace at 350 °C overnight to remove the PMMA scaffold.

Transmission Electron Microscopy and Image Processing. HRTEM was performed using Oxford's JEOL JEM-2200MCO field-emission gun TEM, using a CEOS imaging aberration corrector and an accelerating voltage of 80 kV. A double Wien filter monochromator with a 7 μm slit was used to reduce the energy spread of the electron beam to ~0.21 eV. Data were recorded using a Gatan Ultrascan 4K × 4K CCD camera with 2−5 s acquisition times.

Scanning Transmission Electron Microscopy. A JEM 2100F with a cold field emission source and DELTA-type aberration correctors was operated at 60 kV for STEM experiments. The beam current was estimated at around 40 pA in a 0.1 nm probe.

Heating Holder. To perform variable-temperature experiments, we used both a commercially available *in situ* heating holder from DENS Solutions (SH30-4M-FS) and a JEOL heating holder. In the DENS Solutions holder, heating the sample was achieved by passing a current through a platinum resistive coil imbedded in the TEM chip (DENS Solutions DENS-C-30). The resistance of the platinum coil is monitored in a four-point configuration, and the temperature is calculated using the Callendar−Van Dusen equation (with calibration constants provided by the manufacturer).

Image Processing. Detailed image processing techniques employed are shown within Figure S3 of the Supporting Information.

Conflict of Interest: The authors declare no competing financial interest.

Acknowledgment. J.H.W. thanks the Royal Society and the Sasakawa Fund for support. C.S.A. has received funding from the European Union Seventh Framework Programme under Grant Agreement 312483-ESTEEM2 (Integrated Infrastructure Initiative|3).

Supporting Information Available: Extra TEM images, study of hole opening rate, and image processing techniques employed. This material is available free of charge via the Internet at http://pubs.acs.org.

REFERENCES AND NOTES

1. Nakada, K.; Fujita, M.; Dresselhaus, G.; Dresselhaus, M. S. Edge State in Graphene Ribbons: Nanometer Size Effect and Edge Shape Dependence. *Phys. Rev. B* **1996**, *54*, 17954–17961.
2. Wang, X.; Ouyang, Y.; Li, X.; Wang, H.; Guo, J.; Dai, H. Room-Temperature All-Semiconducting Sub-10-nm Graphene Nanoribbon Field-Effect Transistors. *Phys. Rev. Lett.* **2008**, *100*, 206803.
3. Ezawa, M. Peculiar Width Dependence of the Electronic Properties of Carbon Nanoribbons. *Phys. Rev. B* **2006**, *73*, 045432.
4. Son, Y.-W.; Cohen, M. L.; Louie, S. G. Half-Metallic Graphene Nanoribbons. *Nature* **2006**, *444*, 347–349.
5. Son, Y.-W.; Cohen, M. L.; Louie, S. G. Energy Gaps in Graphene Nanoribbons. *Phys. Rev. Lett.* **2006**, *97*, 216803.
6. Wang, Z. F.; Li, Q.; Zheng, H.; Ren, H.; Su, H.; Shi, Q. W.; Chen, J. Tuning the Electronic Structure of Graphene Nanoribbons through Chemical Edge Modification: A Theoretical Study. *Phys. Rev. B* **2007**, *75*, 113406.
7. Wassmann, T.; Seitsonen, A. P.; Saitta, A. M.; Lazzeri, M.; Mauri, F. Structure, Stability, Edge States, and Aromaticity of Graphene Ribbons. *Phys. Rev. Lett.* **2008**, *101*, 096402.
8. Han, M.; Özyilmaz, B.; Zhang, Y.; Kim, P. Energy Band-Gap Engineering of Graphene Nanoribbons. *Phys. Rev. Lett.* **2007**, *98*, 206805.
9. Ritter, K. A.; Lyding, J. W. The Influence of Edge Structure on the Electronic Properties of Graphene Quantum Dots and Nanoribbons. *Nat. Mater.* **2009**, *8*, 235–242.
10. Akola, J.; Heiskanen, H.; Manninen, M. Edge-Dependent Selection Rules in Magic Triangular Graphene Flakes. *Phys. Rev. B* **2008**, *77*, 193410.
11. Cocchi, C.; Ruini, A.; Prezzi, D.; Caldas, M. J.; Molinari, E. Designing All-Graphene Nanojunctions by Covalent Functionalization. *J. Phys. Chem. C* **2011**, *115*, 2969–2973.
12. Lü, X.; Zheng, Y.; Xin, H.; Jiang, L. Spin Polarized Electron Transport through a Graphene Nanojunction. *Appl. Phys. Lett.* **2010**, *96*, 132108.
13. Cocchi, C.; Prezzi, D.; Ruini, A.; Caldas, M. J.; Molinari, E. Optical Properties and Charge-Transfer Excitations in Edge-Functionalized All-Graphene Nanojunctions. *J. Phys. Chem. Lett.* **2011**, *2*, 1315–1319.
14. Cai, J.; Ruffieux, P.; Jaafar, R.; Bieri, M.; Braun, T.; Blankenburg, S.; Muoth, M.; Seitsonen, A. P.; Saleh, M.; Feng, X.; et al. Atomically Precise Bottom-up Fabrication of Graphene Nanoribbons. *Nature* **2010**, *466*, 470–473.
15. Hämäläinen, S. K.; Sun, Z.; Boneschanscher, M. P.; Uppstu, A.; Ijäs, M.; Harju, A.; Vanmaekelbergh, D.; Liljeroth, P. Quantum-Confined Electronic States in Atomically Well-Defined Graphene Nanostructures. *Phys. Rev. Lett.* **2011**, *107*, 236803.
16. Kobayashi, Y.; Fukui, K.; Enoki, T.; Kusakabe, K.; Kaburagi, Y. Observation of Zigzag and Armchair Edges of Graphite Using Scanning Tunneling Microscopy and Spectroscopy. *Phys. Rev. B* **2005**, *71*, 193406.
17. Tao, C.; Jiao, L.; Yazyev, O. V.; Chen, Y.-C.; Feng, J.; Zhang, X.; Capaz, R. B.; Tour, J. M.; Zettl, A.; Louie, S. G.; et al. Spatially Resolving Edge States of Chiral Graphene Nanoribbons. *Nat. Phys.* **2011**, *7*, 616–620.
18. He, K.; Lee, G.-D.; Robertson, A. W.; Yoon, E.; Warner, J. H. Hydrogen-Free Graphene Edges. *Nat. Commun.* **2014**, *5*, 3040.
19. Girit, Ç. Ö.; Meyer, J. C.; Erni, R.; Rossell, M. D.; Kisielowski, C.; Yang, L.; Park, C.-H.; Crommie, M. F.; Cohen, M. L.; Louie, S. G.; et al. Graphene at the Edge: Stability and Dynamics. *Science* **2009**, *323*, 1705–1708.
20. Liu, Z.; Suenaga, K.; Harris, P.; Iijima, S. Open and Closed Edges of Graphene Layers. *Phys. Rev. Lett.* **2009**, *102*, 015501.
21. Krivanek, O. L.; Chisholm, M. F.; Nicolosi, V.; Pennycook, T. J.; Corbin, G. J.; Dellby, N.; Murfitt, M. F.; Own, C. S.; Szilagyi, Z. S.; Oxley, M. P.; et al. Atom-by-Atom Structural and Chemical Analysis by Annular Dark-Field Electron Microscopy. *Nature* **2010**, *464*, 571–574.
22. Krauss, B.; Nemes-Incze, P.; Skakalova, V.; Biro, L. P.; Klitzing, K.; Von Smet, J. H. Raman Scattering at Pure Graphene Zigzag Edges. *Nano Lett.* **2010**, *10*, 4544–4548.
23. Ni, Z. H.; Chen, W.; Fan, X. F.; Kuo, J. L.; Yu, T.; Wee, A. T. S.; Shen, Z. X. Raman Spectroscopy of Epitaxial Graphene on a SiC Substrate. *Phys. Rev. B* **2008**, *77*, 115416.
24. Kosynkin, D. V.; Higginbotham, A. L.; Sinitskii, A.; Lomeda, J. R.; Dimiev, A.; Price, B. K.; Tour, J. M. Longitudinal Unzipping of Carbon Nanotubes To Form Graphene Nanoribbons. *Nature* **2009**, *458*, 872–876.
25. Jiao, L.; Zhang, L.; Wang, X.; Diankov, G.; Dai, H. Narrow Graphene Nanoribbons from Carbon Nanotubes. *Nature* **2009**, *458*, 877–880.
26. Campos, L. C.; Manfrinato, V. R.; Sanchez-Yamagishi, J. D.; Kong, J.; Jarillo-Herrero, P. Anisotropic Etching and

Nanoribbon Formation in Single-Layer Graphene. *Nano Lett.* **2009**, *9*, 2600–2604.
27. Schäffel, F.; Wilson, M.; Bachmatiuk, A.; Rümmeli, M. H.; Queitsch, U.; Rellinghaus, B.; Briggs, G. A. D.; Warner, J. H. Atomic Resolution Imaging of the Edges of Catalytically Etched Suspended Few-Layer Graphene. *ACS Nano* **2011**, *5*, 1975–1983.
28. Yang, R.; Zhang, L.; Wang, Y.; Shi, Z.; Shi, D.; Gao, H.; Wang, E.; Zhang, G. An Anisotropic Etching Effect in the Graphene Basal Plane. *Adv. Mater.* **2010**, *22*, 4014–4019.
29. Krauss, B.; Nemes-Incze, P.; Skakalova, V.; Biro, L. P.; Klitzing, K. Von; Smet, J. H. Raman Scattering at Pure Graphene Zigzag Edges. *Nano Lett.* **2010**, *10*, 4544–4548.
30. Casiraghi, C.; Hartschuh, A.; Qian, H.; Piscanec, S.; Georgi, C.; Fasoli, A.; Novoselov, K. S.; Basko, D. M.; Ferrari, A. C. Raman Spectroscopy of Graphene Edges. *Nano Lett.* **2009**, *9*, 1433–1441.
31. Schäffel, F.; Wilson, M.; Bachmatiuk, A.; Rümmeli, M. H.; Queitsch, U.; Rellinghaus, B.; Briggs, G. A. D.; Warner, J. H. Atomic Resolution Imaging of the Edges of Catalytically Etched Suspended Few-Layer Graphene. *ACS Nano* **2011**, *5*, 1975–1983.
32. Koskinen, P.; Malola, S.; Häkkinen, H. Evidence for Graphene Edges beyond Zigzag and Armchair. *Phys. Rev. B* **2009**, *80*, 073401.
33. Kim, K.; Coh, S.; Kisielowski, C.; Crommie, M. F.; Louie, S. G.; Cohen, M. L.; Zettl, A. Atomically Perfect Torn Graphene Edges and Their Reversible Reconstruction. *Nat. Commun.* **2013**, *4*, 2723.
34. Lee, G.-D.; Wang, C. Z.; Yoon, E.; Hwang, N.-M.; Ho, K. M. Reconstruction and Evaporation at Graphene Nanoribbon Edges. *Phys. Rev. B* **2010**, *81*, 195419.
35. Stone, A. J.; Wales, D. J. Theoretical Studies of Icosahedral C60 and Some Related Species. *Chem. Phys. Lett.* **1986**, *128*, 501–503.
36. Koskinen, P.; Malola, S.; Häkkinen, H. Self-Passivating Edge Reconstructions of Graphene. *Phys. Rev. Lett.* **2008**, *101*, 115502.
37. Song, B.; Schneider, G. F.; Xu, Q.; Pandraud, G.; Dekker, C.; Zandbergen, H. Atomic-Scale Electron-Beam Sculpting of Near-Defect-Free Graphene Nanostructures. *Nano Lett.* **2011**, *11*, 2247–2250.
38. Lusk, M. T.; Wu, D. T.; Carr, L. D. Graphene Nanoengineering and the Inverse Stone-Thrower-Wales Defect. *Phys. Rev. B* **2010**, *81*, 155444.
39. Kotakoski, J.; Santos-Cottin, D.; Krasheninnikov, A. V. Stability of Graphene Edges under Electron Beam: Equilibrium Energetics *versus* Dynamic Effects. *ACS Nano* **2012**, *6*, 671–676.
40. Robertson, A. W.; Allen, C. S.; Wu, Y. A.; He, K.; Olivier, J.; Neethling, J.; Kirkland, A. I.; Warner, J. H. Spatial Control of Defect Creation in Graphene at the Nanoscale. *Nat. Commun.* **2012**, *3*, 1144.
41. Okada, S. Energetics of Nanoscale Graphene Ribbons: Edge Geometries and Electronic Structures. *Phys. Rev. B* **2008**, *77*, 041408.
42. Liu, Y.; Dobrinsky, A.; Yakobson, B. I. Graphene Edge from Armchair to Zigzag: The Origins of Nanotube Chirality? *Phys. Rev. Lett.* **2010**, *105*, 235502.
43. Chuvilin, A.; Meyer, J. C.; Algara-Siller, G.; Kaiser, U. From Graphene Constrictions to Single Carbon Chains. *New J. Phys.* **2009**, *11*, 083019.
44. Westenfelder, B.; Meyer, J. C.; Biskupek, J.; Kurasch, S.; Scholz, F.; Krill, C. E.; Kaiser, U. Transformations of Carbon Adsorbates on Graphene Substrates under Extreme Heat. *Nano Lett.* **2011**, *11*, 5123–5127.
45. Wu, Y. A.; Fan, Y.; Speller, S.; Creeth, G. L.; Sadowski, J. T.; He, K.; Robertson, A. W.; Allen, C. S.; Warner, J. H. Large Single Crystals of Graphene on Melted Copper Using Chemical Vapor Deposition. *ACS Nano* **2012**, *6*, 5010–5017.